Geoderma 357 (2020) 113943

Contents lists available at ScienceDirect

Geoderma

journal homepage: www.elsevier.com/locate/geoderma

Denitrifying anaerobic methane oxidation in intertidal marsh soils: Occurrence and environmental significance

Yanling Zheng[a,b,c], Lijun Hou[c,*], Feiyang Chen[c], Jie Zhou[c], Min Liu[a,b,**], Guoyu Yin[a,b], Juan Gao[c], Ping Han[a,b,c]

[a] School of Geographic Sciences, East China Normal University, Shanghai 200241, China
[b] Key Laboratory of Geographic Information Science (Ministry of Education), East China Normal University, Shanghai 200241, China
[c] State Key Laboratory of Estuarine and Coastal Research, East China Normal University, Shanghai 200241, China

ARTICLE INFO

Handling Editor: Daniel Said-Pullicino

Keywords:
Denitrifying anaerobic methane oxidation (DAMO)
Nitrogen removal
Community dynamics
Soils
Tidal dynamics
The Yangtze estuary

ABSTRACT

Denitrifying anaerobic methane oxidation (DAMO), consisting of nitrite-dependent DAMO (nitrite-DAMO) and nitrate-dependent DAMO (nitrate-DAMO), has recently been discovered and considered an important link between carbon and nitrogen cycles. In this work, we investigated biodiversity, abundance, and potential methane (CH_4) oxidation activity of nitrite-DAMO bacteria and nitrate-DAMO archaea in intertidal marsh soil cores, based on molecular and stable isotope tracing methods. Results evidenced the co-occurrence and vertical stratification of DAMO bacteria and archaea in intertidal marsh soils, with higher biodiversity of DAMO archaea compared with DAMO bacteria. The abundance of DAMO bacterial *pmoA* gene (8.2×10^5–3.0×10^7 copies g^{-1} dry soil) was approximate to that of DAMO archaeal *mcrA* gene (3.0×10^5–3.9×10^7 copies g^{-1} dry soil) in the intertidal marsh soil cores. Stable isotope experiments showed that DAMO bacteria and archaea were both active in the intertidal marshes, with CH_4 oxidation potential of 0.1–3.8 nmol $^{13}CO_2$ g^{-1} dry soil day^{-1} and 0.1–4.1 nmol $^{13}CO_2$ g^{-1} dry soil day^{-1}, respectively. The relative importance (including the abundance and CH_4 oxidation activity) of DAMO bacteria and archaea showed significant vertical variations, with more contribution by DAMO bacteria at the soil-tidal water interface and soil-groundwater interface layers of the soil cores, which are largely due to the influence of tidal dynamics. In addition to playing an important role as CH_4 sink, DAMO process was also a non-negligible pathway of nitrogen removal in intertidal marsh soils, with an estimated nitrogen removal rate of 0.4–10.1 nmol N g^{-1} dry soil day^{-1}. Overall, these results illustrated the occurrence and environmental significance of DAMO bioprocess in intertidal marshes.

1. Introduction

Methane (CH_4) is a powerful anthropogenic greenhouse gas that contributes approximately 22% to the global warming, second only to carbon dioxide (CO_2) (Dean et al., 2018; Myhre et al., 2013; Wang et al., 2019). Its 100-year global warming potential is 20–30 times that of CO_2 because of its higher efficiency of heat absorption (Myhre et al., 2013). Since the beginning of the industrial era, atmospheric concentrations of CH_4 have increased by 150%, and its emission still continues to increase by approximately 1% per year, consequently exacerbating climate change (Schwietzke et al., 2016). Coastal wetlands, as important ecotones between land and sea, perform vital ecological and environmental functions (Bastviken et al., 2011; Shen et al., 2015). Although coastal wetlands comprise only a small area of the earth's surface, they emit 40 to 160 Tg of CH_4 per year, accounting for 7 to 30% of global annual CH_4 flux (Segarra et al., 2013). The produced CH_4 in wetlands can be removed by microbial processes which mainly includes aerobic CH_4 oxidation catalyzed by aerobic methanotrophs and anaerobic CH_4 oxidation catalyzed by anaerobic methanotrophs (Deng et al., 2016; Sultana et al., 2019; Welte et al., 2016). In wetland soils, oxygen is usually depleted rapidly within a few millimeter depth, leaving the bulk of the soil anoxic (Zheng et al., 2016). Therefore, CH_4 can also be oxidized anaerobically in anoxic soil layers using electron acceptors such as sulfate (SO_4^{2-}) (Knittel and Boetius, 2009), manganese/iron (Beal et al., 2009), and nitrite (NO_2^-)/nitrate (NO_3^-) (Ettwig et al., 2010; Haroon et al., 2013). Recently, a novel CH_4 sink

* Corresponding author at: State Key Laboratory of Estuarine and Coastal Research, East China Normal University, 500 Dongchuan Road, Minhang District, Shanghai 200241, China.
** Correspondence to: M. Liu, School of Geographic Sciences, East China Normal University, 500 Dongchuan Road, Minhang District, Shanghai 200241, China.
E-mail addresses: ljhou@sklec.ecnu.edu.cn (L. Hou), mliu@geo.ecnu.edu.cn (M. Liu).

https://doi.org/10.1016/j.geoderma.2019.113943
Received 31 May 2019; Received in revised form 27 August 2019; Accepted 28 August 2019
Available online 06 September 2019
0016-7061/

linking anaerobic CH_4 oxidation to the reduction of humic fraction of natural organic matter in wetlands was also evidenced (Valenzuela et al., 2017, 2019). In marine environments, sulfate-dependent anaerobic oxidation of methane (sulfate-AOM) has been identified as an important CH_4 sink (Knittel and Boetius, 2009). However, anaerobic oxidation of CH_4 coupled with NO_2^-/NO_3^- reduction is thermodynamically favored over sulfate-AOM in the environments where NO_2^-/NO_3^- and SO_4^{2-} co-existed (Shen et al., 2019). Additionally, in coastal wetlands, reactive nitrogen is highly enriched and rapidly transformed due mainly to the excessive input of anthropogenic nitrogen (Canfield et al., 2010; Hou et al., 2013). Thus, NO_2^- and NO_3^- are very likely to be more important electron acceptors for anaerobic oxidation of CH_4 in coastal wetlands.

Anaerobic oxidation of CH_4 coupled to NO_2^-/NO_3^- reduction, i.e. denitrifying anaerobic methane oxidation (DAMO), is a recently discovered process using NO_2^-/NO_3^- as electron acceptors to oxidize CH_4 (Ettwig et al., 2009, 2010; Raghoebarsing et al., 2006). This process is an important link between the two major global nutrient cycles of carbon and nitrogen (Hu et al., 2014a; Wang et al., 2019), as well as the natural organic matter-dependent anaerobic ammonium oxidation (anammox) process which also interconnects both cycles (Rios-Del Toro et al., 2018). *Candidatus* Methylomirabilis oxyfera (hereinafter abbreviated as *M. oxyfera*), belonging to the bacterial NC10 phylum, was the first discovered microorganism that can perform nitrite-dependent DAMO process (nitrite-DAMO) via utilizing NO_2^- as the electron acceptor to anaerobically oxidize CH_4 (Ettwig et al., 2010). This microorganism exhibited an intra-aerobic metabolism in which nitric oxide was hypothesized to be dismutated to oxygen and dinitrogen gas, and the produced oxygen could subsequently be used by the canonical particulate methane monooxygenase encoded by *pmoCAB* gene to oxidize CH_4 (Ettwig et al., 2010). Later, NC10 bacteria *Candidatus* Methylomirabilis Sinica (hereinafter abbreviated as *M. sinica*) was also reported to perform the same function (He et al., 2016a). Nitrate-dependent DAMO process (nitrate-DAMO) was found to be catalyzed by a new type of archaea belonging to the ANME-2d clade, *Candidatus* Methanoperedens nitroreducens (hereinafter abbreviated as *M. nitroreducens*), which is capable of using NO_3^- as the final electron acceptor to oxidize CH_4 by reverse methanogenesis pathway (Haroon et al., 2013). This microorganism can transform NO_3^- into NO_2^- which can be used by nitrite-DAMO bacteria, whereas the latter can only use NO_2^- instead of NO_3^- (Ettwig et al., 2010; Haroon et al., 2013). Therefore, nitrite-DAMO bacteria and nitrate-DAMO archaea may form a cooperative relationship to coexist in the natural environments (Wang et al., 2019).

Since their discovery in 2010, nitrite-DAMO bacteria have been detected in various natural ecosystems including lakes (Hu et al., 2014a; Shen et al., 2015), rivers (Shen et al., 2014a), estuaries (Shen et al., 2014b), paddy fields (Hu et al., 2014a; Zhou et al., 2014), coastal wetlands (Shen et al., 2016; Wang et al., 2017, 2019), and marine ecosystems (Chen et al., 2014; Padilla et al., 2016). Nevertheless, the research on nitrate-DAMO archaea in natural habitats is still very limited so far, and their CH_4 removal potential also remains to be explored. Intertidal marsh, as an important component of coastal wetlands, performs as a large source of greenhouse gas CH_4 and has also suffered from a substantial loading of anthropogenic nitrogen (Kintisch, 2013; Zheng et al., 2016). Hence, a deeper understanding of how CH_4 oxidation and nitrogen removal processes are coupled in the intertidal marshes is required. As yet, the community dynamics of DAMO bacteria and archaea, their contributions to carbon and nitrogen cycling, as well as the underlying controlling mechanisms in intertidal marshes remain unclear.

Unlike other wetland ecosystems, the intertidal marsh soils are exposed and submerged alternately during tidal cycles, giving rise to rhythmic material fluxes between the oxygenated tidal water and marsh surface soil (called soil-tidal water interface) (Santos et al., 2012; Urish and McKenna, 2004; Zheng et al., 2016). Additionally, tidal dynamics induce periodic fluctuations of the groundwater table, which in turn contributes to the pulsed input of oxygenated water, as well as other solutes and particles into deeper marsh soil (called soil-groundwater interface) (Santos et al., 2012; Urish and McKenna, 2004; Zheng et al., 2016). These tidal forces are evidenced to change the marsh soil physicochemical conditions and play an important role in controlling denitrification and anammox processes in intertidal marsh soil cores in our previous study (Zheng et al., 2016). Therefore, the tidal dynamics are hypothesized to affect the community diversity and activity of DAMO microbes in intertidal marshes, as denitrification is a potential nitrite source for DAMO bacteria, and anammox bacteria are syntrophic and competitive partners to DAMO archaea and DAMO bacteria, respectively (Haroon et al., 2013; Hu et al., 2015). Hence, in the present study, we aimed to investigate the vertical changes of nitrite- and nitrate-dependent methanotrophs, and their importance in CH_4 oxidation and nitrogen removal in the intertidal marshes of the Yangtze Estuary, which is one of the largest estuaries in the world and contains extensive intertidal marshes, using molecular and ^{13}C isotope-tracer techniques. This study is of great significance to deepen the understanding of the coupled carbon and nitrogen transformations in the intertidal ecosystems.

2. Materials and methods

2.1. Study area and field sampling

The study area was located in the Chongming eastern intertidal flat, which is the largest and most developed intertidal wetland in the Yangtze Estuary (Fig. S1). The tides are semi-diurnal, with a typical tidal range of 0.4–4.6 m. At the study area, *Phragmites communis*, *Scirpus triqueter* and other salt marsh vegetation are distributed in patches. In the present study, six soil cores (7.2-cm diameter and 100-cm depth) were collected with PVC corers from the unvegetated intertidal area (to exclude the effect of plant roots) in October 2017. The soil cores were sealed with butyl-rubber plugs and transported to the laboratory within 4 h. In the laboratory, they were sliced every 5 cm under helium atmosphere, and sub-soils from the same depth were mixed to form one composite sample. Each sample was divided into two parts: one for immediate determination of potential DAMO rate and soil physicochemical characteristics, and the other stored at −20 °C for later molecular analysis.

2.2. Determination of environmental parameters

Soil salinity and pH were measured using salinity meter (YSI Model 30, Ohio) and pH meter (Mettler-Toledo, Switzerland), respectively, after soils were mixed with CO_2-free deionized water (w:v = 1:2.5) (Hou et al., 2013). Soil redox potential (Eh) was determined by Eh Automatic Analyzer (FJA-6 ORP, Chuan-Di, Nanjing, China) (Zheng et al., 2016). Soil water content was calculated via the weight loss of a certain amount of wet soil dried under 80 °C (Zheng et al., 2014). Soil grain-size composition was analyzed with a Beckman Coulter LS13320 laser granulometer (USA) (Zheng et al., 2014). Soil NH_4^+, NO_2^-, and NO_3^- were extracted with 2 M KCl and measured spectrophotometrically using a continuous-flow nutrient analyzer (SAN plus, Skalar AnalyticalB.V., the Netherlands) with detection limits of 0.5 μM for NH_4^+-N, and 0.1 μM for NO_2^--N and NO_3^--N (Hou et al., 2013). For determination of soil organic carbon (OC), approximately 0.2 g soil was digested with 5 mL of 0.8 M $K_2Cr_2O_7$ and 5 mL of concentrated H_2SO_4 in an oil-bath at 170–180 °C for 5 min. Excess Cr (VI) was then back titrated with 0.2 M ferrous ammonium sulfate ($FeSO_4(NH_4)_2SO_4.6H_2O$) using diphenylamine as an indicator, and soil OC content can therefore be calculated on the basis of the consumption of ferrous ion (Zheng et al., 2014). Reactive iron content in soil was measured via colorimetric method (Haese et al., 1997; Wallmann et al., 1993). Briefly, reactive iron was extracted from 0.5 g of fresh soil via agitation

with 30 mL of 0.5 M anoxic HCl solution for 1 h. The content of total iron including ferrous iron Fe(II) + ferric iron Fe(III) was then determined with a 1, 10-phenanthroline and 1% (w/v) hydroxylamine hydrochloride assay, followed by the Fe(II) directly via a 1, 10-phenanthroline method. Fe(III) content was then calculated as the difference between the total iron and Fe(II) contents (Haese et al., 1997; Wallmann et al., 1993). Soil SO_4^{2-} was determined by $BaSO_4$ turbidimetric method after it was extracted using $Ca(H_2PO_4)_2$ (Ajwa and Tabatabai, 1993). All these environmental parameters were analyzed in triplicate.

To determine CH_4 concentrations, a known amount (approximately 3 g) of fresh soil was subsampled and immediately immersed into 20 mL serum vials containing a saturated NaCl solution under helium conditions (Winkel et al., 2018). Serum vials were sealed with butyl-rubber stoppers and a crimp seal, and were shaken immediately and stored upside down for at least 24 h to drive the CH_4 into the headspace. Headspace CH_4 concentration was measured by gas chromatograph (GC-2014, Shimadzu) equipped with a flame ionization detector (Wang et al., 2019). The amount of CH_4 in the vials was calculated from the headspace concentrations and the volume of liquid in the bottles (Supplementary text 1). CH_4 concentrations are reported relative to soil pore water volume based on soil water content (Winkel et al., 2018).

2.3. DNA extraction and gene amplification

Total genomic DNA of each sample was extracted from approximately 0.25 g wet soil using Powersoil™ DNA Isolation Kits (MOBIO, USA). Triplicate qualified DNA extracts were pooled and used for the down-stream molecular analyses. In the present study, the alpha subunit of the particulate methane monooxygenase gene (*pmoA*) was used to identify the nitrite-DAMO bacteria (*M. oxyfera*-like bacteria) (Luesken et al., 2011), while the alpha subunit of the methyl-coenzyme M reductase gene (*mcrA*) was used to investigate the nitrate-DAMO archaea (*M. nitroreducens*-like archaea) (Vaksmaa et al., 2017a). DAMO bacterial *pmoA* gene was amplified using a nested polymerase chain reaction (PCR) method, consisting of an initial PCR amplification with primers A189_b/cmo682 followed by a second PCR with primers cmo182/cmo568, which results in a final 389 bp PCR product (Luesken et al., 2011). PCR amplification of *mcrA* gene (1191 bp) from DAMO archaea was carried out with primers McrA169F/McrA1360R (Vaksmaa et al., 2017a). Detailed PCR protocols used in this study are given in Table S1. Appropriately-sized fragments containing the targeted genes were purified and cloned using the TOPO-TA cloning kit (Invitrogen, USA). Positive clones were selected by blue-white screening for further analysis.

2.4. Sequencing and phylogenetic analysis

Selected positive clones were sequenced on an ABI Prism genetic analyzer (Applied Biosystems, Canada). Possible chimeras were checked using the QIIME 1.9.0 software package (Caporaso et al., 2010). Subsequently, the qualified nucleic acid sequences with > 97% identities were defined as one operational taxonomic unit (OTU) by software Mothur (version 1.35.1) using the furthest neighbor method (Schloss et al., 2009). MEGA 7.0.21 program was used for the construction of neighbor-joining phylogenetic tree (Kumar et al., 2016), and the robustness of tree topology was assessed by bootstrap analysis (1000 replicates). The biodiversity indicators (Shannon-Wiener and Simpson) and species richness Chao1 estimator were calculated using QIIME 1.9.0 (Caporaso et al., 2010). QIIME 1.9.0 was also used to construct the rarefaction curves for the *pmoA* and *mcrA* gene clone libraries, as well as to calculate the UniFrac distances between each pair of the clone libraries. Coverage of the constructed clone libraries was estimated by the ratio of the obtained OTU number to Chao1 estimator (Mohamed et al., 2010). The unique *pmoA* and *mcrA* sequences obtained in the present study have been deposited in GenBank with accession numbers of MK887934-MK888035 and MK888036-MK888208, respectively.

2.5. Quantitative PCR assay

Real-time quantitative PCR (qPCR) was performed with the ABI 7500 to determine the abundance of nitrite-DAMO bacterial *pmoA* gene and nitrate-DAMO archaeal *mcrA* gene in the soils using primers cmo182/cmo568 (Luesken et al., 2011) and McrA159F/McrA345R (Vaksmaa et al., 2017a), respectively. Detailed information for the primers and qPCR protocols used in the study is shown in Table S1. Standard curves were constructed using a series of tenfold dilutions of the standard plasmids (known copy number) containing the targeted genes. To lower the possibility of over-estimation, melting curves and gel electrophoreses were both performed. In addition, negative controls without any DNA template addition were also conducted in all the amplification reactions.

2.6. Measurement of potential DAMO rates

Potential rates of DAMO bacteria and archaea were measured using slurry experiments in combination with ^{13}C isotope-tracing technique, as previously described (Hu et al., 2014a; Wang et al., 2019). Briefly, slurries were prepared with He-purged filtered seawater and fresh soils at a volume ratio of 3:1 (water/soil) and then were transferred to He-flushed, 120-mL glass vials. The slurries were pre-incubated under anaerobic conditions for at least 30 h to remove the residual NO_x^- and O_2. The slurries were subsequently split into different treatment groups: (a) $^{13}CH_4$ (^{13}C at 99%), (b) $^{13}CH_4 + NO_2^-$, and (c) $^{13}CH_4 + NO_3^-$. Subsequently, 50 μL of He-purged NO_2^-/NO_3^- stock solution was injected through the septa into each vial, resulting in a final concentration of 0.5 mM of NO_2^- in group (b) and 5 mM NO_3^- in group (c) (Fig. S2). Immediately after that, $^{13}CH_4$ was injected into these vials, resulting in a final concentration of 1% (v/v) in the headspace. Additional slurries without any additions were also left as control to determine the background $^{13}CO_2$ during incubation. Each treatment was conducted in triplicate. All the slurries were incubated at in situ temperature in the dark with gentle shaking at 120 rpm. The incubation was inhibited by injecting 50% $ZnCl_2$ solution after 1 day (Fig. S3). The production of $^{13}CO_2$ in the headspace of each vial was measured directly using Delta V Advantage Isotope Ratio Mass Spectrometer (IRMS, Thermo Fisher Scientific). The total amount of produced $^{13}CO_2$ in the headspace and liquid of each vial was quantified according to the equation reported by He et al. (2016b). The potential rates of DAMO, nitrite-DAMO, and nitrate-DAMO were calculated as previously described (He et al., 2016b; Wang et al., 2019). Specifically, the potential DAMO rate was measured by subtracting the production of $^{13}CO_2$ during the incubation amended with $^{13}CH_4$ (group a) from the production of $^{13}CO_2$ during the incubation amended with $^{13}CH_4 + NO_3^-$ (group c). Nitrite-DAMO rate was determined by subtracting the production of $^{13}CO_2$ during the incubation amended with $^{13}CH_4$ (group a) from the production of $^{13}CO_2$ during the incubation amended with $^{13}CH_4 + NO_2^-$ (group b). Nitrate-DAMO rate was estimated by subtracting the production of $^{13}CO_2$ during the incubation amended with $^{13}CH_4 + NO_2^-$ (group b) from the production of $^{13}CO_2$ during the incubation amended with $^{13}CH_4 + NO_3^-$ (group c).

2.7. Statistical analysis

General statistical analysis was conducted using statistical product and service solutions 18.0 software (SPSS). Pearson's correlation was used to evaluate the relationships among the abundance and activity of DAMO microorganisms and environmental variables. One-way ANOVA was adopted to compare the variations of DAMO dynamics in the intertidal marsh soils. In this study, the statistical analyses were considered significant at $P < 0.05$.

3. Results

3.1. Physicochemical characteristics of intertidal marsh soil cores

Salinity of the intertidal marsh soil cores ranged between 0.2 and 1.3‰, which showed a decrease trend from the soil-tidal water interface down to soil-groundwater interface (Fig. S4). Soil pH, in the range of 8.05–8.34, also tended to decrease with soil depth. The highest Eh value was detected in the surface soil (413 mV), and then it decreased to the lowest value (183 mV) at around 40 cm (supplementary text 2). However, it increased again at deeper layers, and increased up to 362 mV at the soil-groundwater interface. Soils along the entire cores were mainly composed of silt (69.0–75.6%) with smaller amounts of clay (13.2–23.1%) and sand (7.4–16.3%). The maximal NO_3^- concentrations (6.44–10.75 μg N g^{-1} dry soil) were detected at the surface layers (0–10 cm), then they decreased to 0.43–3.37 μg N g^{-1} dry soil down to 100 cm soil depth. NO_2^- concentrations remained relatively low (0.01–0.06 μg N g^{-1} dry soil) in the whole intertidal marsh soil cores. NH_4^+ ranged between 10.85 and 35.89 μg N g^{-1} dry soil, and relatively high concentrations generally appeared at the soil-groundwater interface. Higher concentrations of OC were detected at the subsurface layers of 10–20 cm (1.61–2.10%), then they showed a decrease trend down to 80 cm (0.56%), after which a slight increase was observed (0.58–1.17%). Soil SO_4^{2-} decreased gradually from the top layer (0.33 mg g^{-1}) down to around 60 cm soil depth (0.02 mg g^{-1}), however at the soil-groundwater interface layer below 75 cm, it increased again up to 0.25 mg g^{-1}. Fe (III) ranged between 1.01 and 1.57 mg g^{-1}, with a depth distribution pattern similar to SO_4^{2-}. Nevertheless, Fe(II) concentrations (0.57–1.74 mg g^{-1}) tended to be higher in the middle marsh soil layers. The vertical distribution of CH_4 in soil pore water was relatively complicated, and showed three main peaks at around 20 cm, 60 cm, and 80 cm depths with values of up to 3.75 μM, 3.87 μM, and 5.02 μM, respectively.

3.2. Diversity and phylogenetic analysis of DAMO bacteria

DAMO bacteria in the intertidal marsh soil cores were successfully detected with a nested PCR assay based on the *pmoA* gene. Three *pmoA* clone libraries were constructed in the present study to investigate and compare the community composition and diversity of DAMO bacteria at the surface (0–20 cm), middle (40–60 cm), and deep (80–100 cm) layers of the soil cores, based on the observed vertical profiles of the physicochemical characteristics of the intertidal cores (Fig. S4). A total of 243 *pmoA* clones were sequenced, which showed 86.7–100% sequence similarity among each other and were divided into 6 OTUs based on a 3% divergence in nucleotides (Table 1). These observed OTUs exhibited 88.5–95.6% sequence identity to *Candidatus* Methylomirabilis oxyfera (FP565575), and 84.6–86.9% sequence identity to *Candidatus* Methylomirabilis Sinica (KT443986). In detail, 4, 3, and 2 OTUs were detected in the surface, middle, and deep clone libraries, respectively, and the diversity of DAMO bacteria also showed a decrease trend with soil depth based on the Shannon-Wiener and Simpson indicators, as well as the rarefaction analysis (Table 1 and Fig. S5). Phylogenetic analysis of *pmoA* gene showed that two distinctive clusters were retrieved (Fig. 1). *PmoA* cluster 1 was affiliated with M. oxyfera with 92.1–95.6% sequence identity, and it was also closely related to *pmoA* sequences recovered from other depositional environments such as the Qiantang River sediment (KC503650) (Shen et al., 2014a), Miyun Reservoir sediment (KX423170), and Dongjiang River sediment (KX001174) (Long et al., 2017) with 96.4–99.2% gene identity (Fig. 1a). The majority of the *pmoA* clones retrieved from the middle (88%) and the soil-groundwater interface (100%) layers were affiliated to this cluster, while only 10% of the surface layer *pmoA* sequences were included (Fig. 1b). *PmoA* cluster 2 showed relatively lower identity (88.5–89.7%) with M. oxyfera, however it was affiliated closely (97.9–99.7%) with DAMO bacterial *pmoA* clones retrieved from freshwater sediments (KR337556, KU301590) (Fig. 1a). Sequences affiliated to this cluster were mainly retrieved from the surface layer of the intertidal marsh soil cores (91%), while the remaining 9% were detected at the middle soil layer (Fig. 1c).

3.3. Diversity and phylogenetic analysis of DAMO archaea

DAMO archaea in the intertidal marsh soils were successfully detected based on *mcrA* gene. A total of 92, 80, and 89 qualified DAMO archaeal *mcrA* clones were obtained from the surface (0–20 cm), middle (40–60 cm), and deep (80–100 cm) layers of the soil cores, respectively, which showed 73–100% sequence similarity among each other (Table 1). In each individual clone library, 8 to 19 OTUs occurred, as defined by 3% divergence in nucleotides. Based on the Shannon-Wiener and Simpson indicators, the diversity of DAMO archaea was significantly higher than that of DAMO bacteria ($P < 0.05$) (Table 1), and it was consistent with the result of the rarefaction analysis (Figs. S5 and S6). In contrast to DAMO bacteria, the highest diversity of DAMO archaea was detected at the soil-groundwater interface layer (Table 1). Phylogenetic analysis showed that 97.7% of the obtained *mcrA* gene clones were affiliated to known DAMO archaea of *M. nitroreducens* (JMIY01000002) and *Candidatus* Methanoperedens sp. (LKCM01000102) with as high as 90.3% and 94.0% gene identity, respectively. They also showed high gene identity (up to 97.8%) with *mcrA* sequences retrieved from river sediment (KX290024) (Vaksmaa et al., 2017a), paddy soil (KX290035) (Vaksmaa et al., 2017a), and enrichment culture of freshwater sediment (EU495304) (Ettwig et al., 2008).

Based on the constructed *mcrA* gene phylogenetic tree, 4 distinctive clusters were retrieved (Fig. 2). *McrA* cluster 1, containing 24 out of the observed 33 OTUs, was affiliated with *Candidatus* Methanoperedens sp. with up to 94.0% sequence identity. This cluster dominated all the *mcrA* gene clone libraries retrieved from the surface (71.7%), middle (85.0%), and deep (78.7%) layers of the soil cores (Fig. 2b). Five OTUs

Table 1
Diversity characteristics of nitrite-DAMO bacterial *pmoA* gene clone libraries and nitrate-DAMO archaeal *mcrA* gene clone libraries.

Gene	Sample	No. of clones	OTUs[a]	Chao1[b]	Shannon-Wiener[c]	1/Simpson[d]	Coverage (%)[e]
pmoA	Surface	100	4	4.0	0.52	1.37	100
	Middle	73	3	3.0	0.44	1.32	100
	Deep	70	2	2.0	0.42	1.32	100
mcrA	Surface	92	15	15.0	2.52	12.10	100
	Middle	80	8	8.8	1.45	3.02	91
	Deep	89	19	20.5	2.79	17.40	93

[a] OTUs were defined at 3% nucleotide acid divergence.
[b] Nonparametric statistical predictions of total richness of OTUs based on distribution of singletons and doubletons.
[c] Shannon-Wiener diversity index. A higher number represents more diversity.
[d] Reciprocal of Simpson's diversity index. A higher number represents more diversity.
[e] Percentage of coverage: percentage of observed number of OTUs divided by Chao1 estimate.

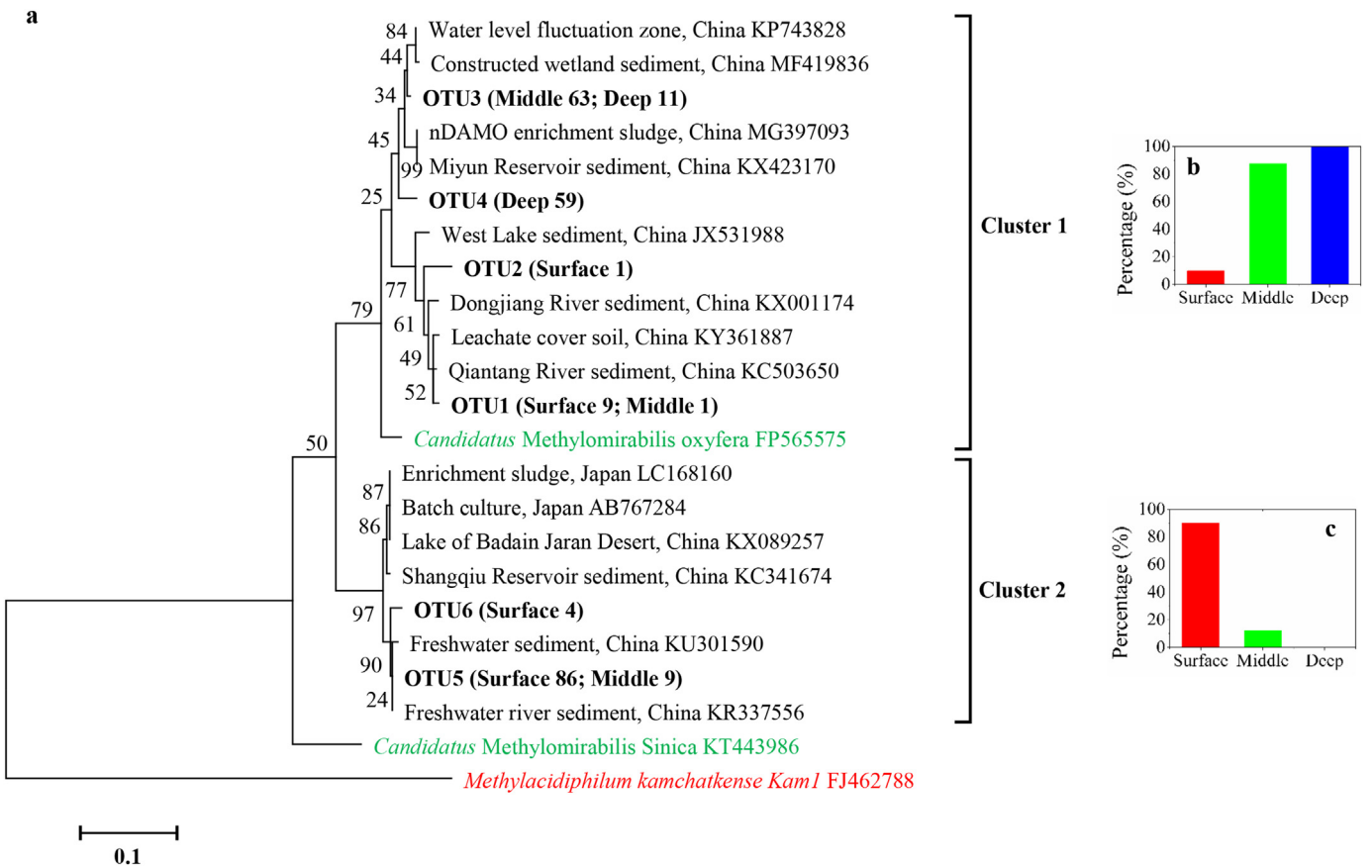

Fig. 1. Neighbor-Joining phylogenetic tree showing the phylogenetic affiliations of nitrite-DAMO bacterial *pmoA* gene sequences recovered from the intertidal marsh soils of the Yangtze Estuary (a), and the percentages of sequences in each sample fall into cluster 1 (b) and cluster 2 (c), respectively. The bootstrap valves > 50% (1000 replicates) are shown at the branch nodes. The scale indicates the number of nucleotide substitutions per site. GenBank accession numbers are shown for sequences from other studies. Numbers in parentheses followed each OTU (in bold) indicate the number of sequences recovered from the surface, middle, and deep layers of the soil cores. Known nitrite-DAMO bacteria are shown in green. *Methylacidiphilum kamchatkense* (in red) is used as the out-group. Evolutionary analyses were conducted in MEGA7. (For interpretation of the references to color in this figure legend, the reader is referred to the web version of this article.)

was affiliated to cluster 2, which showed up to 90.3% gene identity with *M. nitroreducens* (Fig. 2a). The *mcrA* clones of this cluster accounted for 12.0%, 1.3%, and 18.0% of the surface, middle, and deep layer clone libraries, respectively (Fig. 2c). Another 3 OTUs formed cluster 3, which was related most closely to *M. nitroreducens* with up to 88.5% sequence identity, while no more similar gene sequences were detected in other environments so far. The *mcrA* clones of this cluster accounted for 9.8%, 13.8%, and 3.4% of the surface, middle, and deep layer clone libraries, respectively (Fig. 2d). Only one OTU was affiliated to cluster 4, which showed even lower similarity with *M. nitroreducens* (with 76.3% sequence identity) and *Candidatus* Methanoperedens sp. (with 74.1% sequence identity) (Fig. 2a). Nevertheless, it was affiliated closest with *mcrA* clones retrieved from other environments such as the sediment of Lei-Gong-Huo mud volcano (JX648565, with 92.4% sequence identity) (Wang et al., 2014) and the subsurface sediment of Marennes-Oléron Bay (AM942098, with 91.7% sequence identity) (Roussel et al., 2009). *McrA* clones of this cluster were only found at the surface layer but not at the middle and soil-groundwater interface layers (Fig. 2e).

3.4. Abundance of DAMO bacteria and archaea

Abundances of DAMO bacteria and DAMO archaea in the intertidal marsh soil cores were determined using qPCR technique. Melting-curve analyses showed only one peak at 87.4 °C and 83.3 °C for DAMO bacterial *pmoA* gene and DAMO archaeal *mcrA* gene, respectively, confirming that the fluorescent signals were derived from specific qPCR products. Significantly linear relationships were obtained between the threshold cycle (C_T) and the log value of copy number for both genes (r^2 = 0.9995 for *pmoA* and 0.9999 for *mcrA*). In addition, the qPCR amplification efficiencies were 92.3% and 90.7% for *pmoA* and *mcrA* genes, respectively, in the present study. The qPCR results showed that, the numbers of DAMO bacterial *pmoA* gene and DAMO archaeal *mcrA* gene were observed between 8.2×10^5 and 3.0×10^7 copies g^{-1} (dry weight, the same hereinafter), and between 3.0×10^5 and 3.9×10^7 copies g^{-1}, respectively, without significant difference ($P > 0.05$) (Fig. 3). The abundance of DAMO bacteria exhibited an overall decrease trend with soil depth ($P < 0.01$). However, the highest DAMO archaea number was detected at the middle layer of 45–50 cm. The ratio of *pmoA* gene copy number of DAMO bacteria to *mcrA* gene copy number of DAMO archaea ranged between 0.03 and 5.79, and the relative abundance of DAMO bacteria and archaea showed a significant vertical variation along the soil profile (Fig. S7a). The abundance of DAMO bacteria tended to be greater than that of DAMO archaea at the 0–40 cm depth as well as at the soil-groundwater interface, while DAMO archaea tended to be more abundant than DAMO bacteria at the middle layers (Fig. 3 and S7a).

3.5. Potential DAMO rates

The ^{13}C stable isotope tracing method was used to determine the anaerobic CH_4 oxidation activity of DAMO microorganisms in the intertidal marsh soil cores. During the incubation spiked with $^{13}CH_4$ only (group a), no significant production of $^{13}CO_2$ was measured at all soil

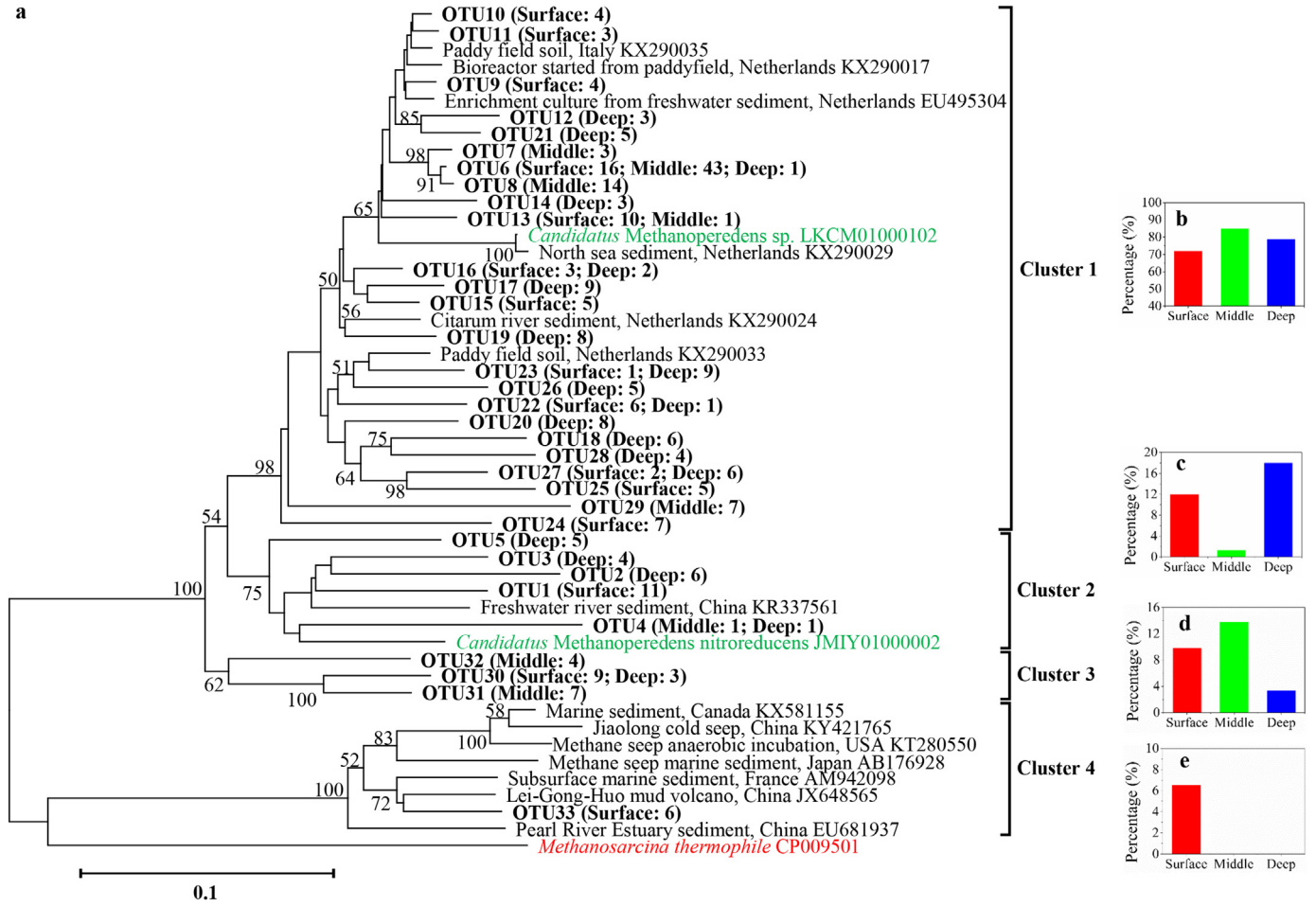

Fig. 2. Neighbor-Joining phylogenetic tree showing the phylogenetic affiliations of nitrate-DAMO archaeal *mcrA* gene sequences recovered from the intertidal marsh soils of the Yangtze Estuary (a), and the percentages of sequences in each sample fall into cluster 1 (b), cluster 2 (c), cluster 3 (d), and cluster 4 (e), respectively. The bootstrap valves > 50% (1000 replicates) are shown at the branch nodes. The scale indicates the number of nucleotide substitutions per site. GenBank accession numbers are shown for sequences from other studies. Numbers in parentheses followed each OTU (in bold) indicate the number of sequences recovered from the surface, middle, and deep layers of the soil cores. Known nitrate-DAMO archaea are shown in green. *Methanosarcina thermophile* (in red) is used as the out-group. Evolutionary analyses were conducted in MEGA7. (For interpretation of the references to color in this figure legend, the reader is referred to the web version of this article.)

layers (similar to the control group) (Fig. S8), showing that the ambient nitrite, nitrate, O_2, and other possible electron acceptors (e.g. SO_4^{2-}, manganese/iron, and humic substances) in the slurries were consumed within the preincubation. During the incubation spiked with $^{13}CH_4$ + NO_2^- (group b) or $^{13}CH_4$ + NO_3^- (group c), significant productions of $^{13}CO_2$ were detected (Fig. S8), confirming the occurrence of DAMO. The activities of DAMO bacteria and DAMO archaea could thereby be obtained on the basis of the production of $^{13}CO_2$ within these incubations.

Results showed that the potential DAMO rates ranged between 0.3 and 7.0 nmol $^{13}CO_2$ g^{-1} dry soil day^{-1} (dry weight, the same hereinafter), exhibiting an overall decrease trend with soil depth ($P < 0.05$), with the highest activity observed at the top layer of 0–5 cm (Fig. 4a). However, an activity peak (4.6 nmol $^{13}CO_2$ g^{-1} dry soil day^{-1}) was also occurred at the 45–50 cm depth (Fig. 4a), where both the highest abundance and the highest activity of DAMO archaea were recorded (Figs. 3 and 4b). The potential nitrite-DAMO and nitrate-DAMO rates were in the range of 0.1–3.8 nmol $^{13}CO_2$ g^{-1} dry soil day^{-1} and 0.1–4.1 nmol $^{13}CO_2$ g^{-1} dry soil day^{-1}, respectively, without significant difference ($P > 0.05$) (Fig. 4b). It was estimated that the nitrogen removal rates ranged between 0.4 and 10.1 nmol N g^{-1} day^{-1}, according to the stoichiometric relation of CH_4 and NO_2^- in the DAMO reaction (3,8) (Fig. S9). In the intertidal marsh soil cores, DAMO bacteria averagely contributed 57% to the CH_4 oxidation during the DAMO process, slightly higher than that of DAMO archaea (43%). The ratio of nitrite-DAMO to nitrate-DAMO rates ranged between 0.05 and 12.51, and showed significant vertical variation along the soil profile (Fig. S7b). The potential nitrite-DAMO rate tended to be higher than that of nitrate-DAMO at the upper 45 cm depth as well as at the soil-groundwater interface, whereas the potential nitrate-DAMO rate tended to be higher at the middle layer (Fig. S7b). This result was consistent with the depth distribution of the relative abundance of DAMO bacteria and archaea (Fig. S7a). Assuming that each cell had equal activity and contained one *pmoA* or *mcrA* gene copy, and that all obtained microbial sequences derived from active microbes, the estimated cell-specific rate of DAMO bacteria varied between 0.02 and 1.00 fmol $^{13}CO_2$ $cell^{-1}$ day^{-1}, while an approximate cell-specific rate was also observed for DAMO archaea (0.01–0.88 fmol $^{13}CO_2$ $cell^{-1}$ day^{-1}).

3.6. Potential controlling factors of DAMO process

The potential effects of environmental factors on the microbial mediated DAMO process in the intertidal marsh soils were analyzed (Fig. 5 and Table S2). Results showed that the abundance of DAMO bacterial *pmoA* gene was positively correlated with salinity, pH, Eh, NO_3^-, SO_4^{2-}, and reactive iron contents ($P < 0.05$), while the DAMO

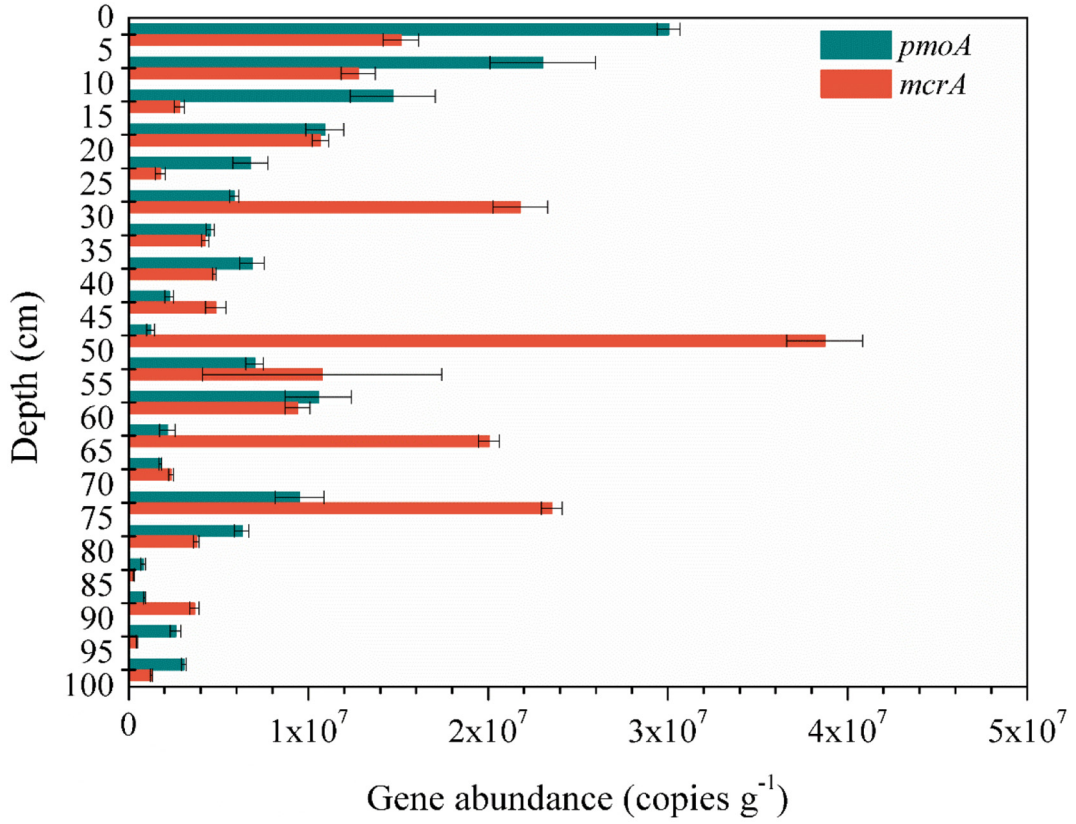

Fig. 3. The abundance of DAMO bacterial *pmoA* gene and DAMO archaeal *mcrA* gene in the intertidal marsh soil cores collected from the Yangtze Estuary. Error bars indicate standard deviations (n = 3).

archaeal *mcrA* gene abundance was only significantly correlated with the soil grain size among all the analyzed environmental parameters ($P < 0.05$). The vertical distribution of DAMO rate was positively correlated with salinity and pH ($P < 0.01$), and it was also negatively correlated with CH_4 in the soil pore water and Fe(II) content ($P < 0.05$). Nitrite-DAMO rate was related to salinity, pH, SO_4^{2-}, NH_4^+, and reactive iron contents ($P < 0.05$), while no significant correlations were detected between nitrate-DAMO rate and measured environmental factors in the present study ($P > 0.05$). In addition, a significant correlation was observed between nitrite-DAMO rate and DAMO bacterial *pmoA* gene abundance ($P < 0.01$), and the activity and abundance of DAMO archaea was also found to be correlated ($P < 0.05$) (Fig. 5). However, the total DAMO rate was only related to DAMO bacterial *pmoA* gene abundance ($P < 0.01$), but not to the DAMO archaeal *mcrA* gene abundance ($P > 0.05$) (Fig. 5).

4. Discussion

In the present study, the co-occurrence of nitrite- and nitrate-dependent DAMO bioprocesses in intertidal marsh soils of the Yangtze Estuary was evidenced by molecular and stable isotope tracing assays. *PmoA* and *mcrA* gene sequence analyses showed the presence and

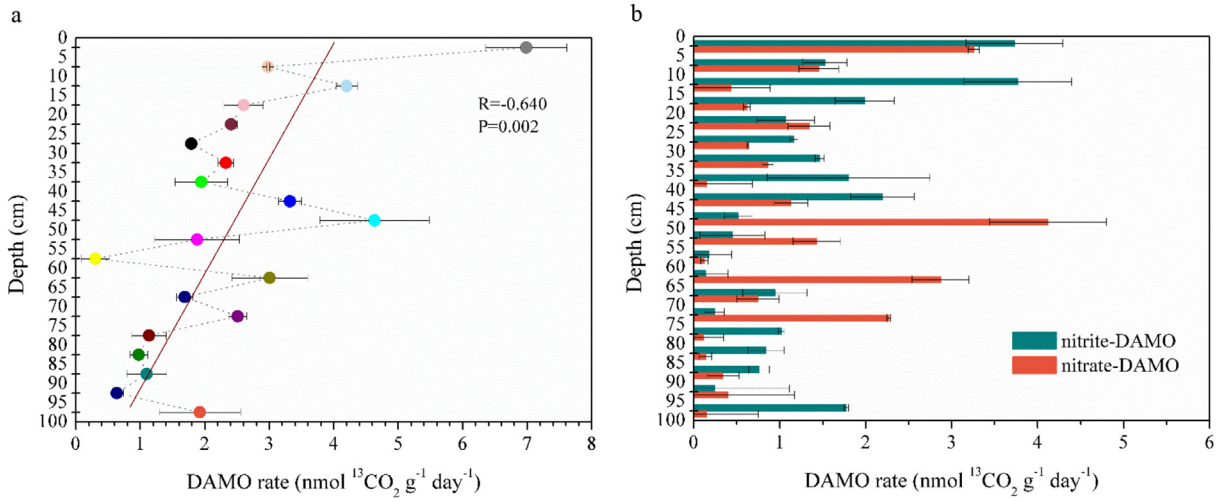

Fig. 4. The total DAMO potential (a) and the nitrite-DAMO and nitrate-DAMO activity (b) in the intertidal marsh soil cores collected from the Yangtze Estuary. Error bars indicate standard deviations (n = 3).

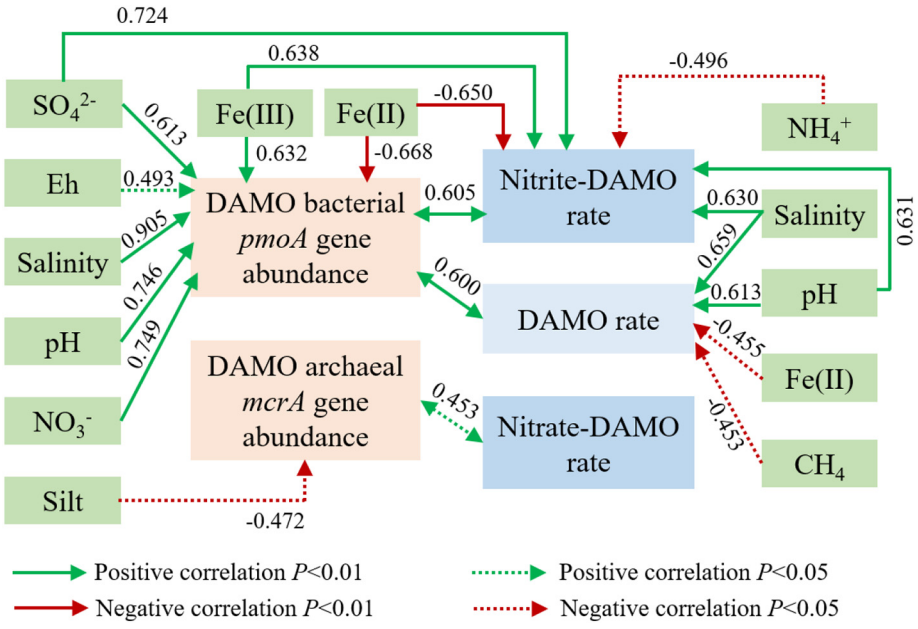

Fig. 5. Pearson's correlation coefficients showing the relationships of environmental factors with the abundance and activity of DAMO microbes in the intertidal marsh soil cores. Data represent the Pearson's correlation coefficients. Solid lines represent statistical significant at $P = 0.01$; dashed lines represent statistical significant at $P = 0.05$; green lines represent positive correlations; and red lines represent negative correlations. (For interpretation of the references to color in this figure legend, the reader is referred to the web version of this article.)

biodiversity of DAMO bacteria and archaea, respectively, and qPCR illustrated their abundance and vertical distribution along the soil cores. The potential CH_4 oxidation activity of DAMO bacteria and archaea in the intertidal soil cores were further revealed based on the ^{13}C stable isotope trace experiment. This study demonstrated the microbiological and environmental significance of anaerobic CH_4 sink coupled with denitrification in the intertidal marshes.

DAMO bacterial *pmoA* gene has been successfully detected in various natural environments, such as lakes (Deutzmann and Schink, 2011; Hu et al., 2014a; Kojima et al., 2012), rivers (Shen et al., 2014a), and estuaries (Shen et al., 2014b). In this study, 2–4 *pmoA* gene OTUs based on a 3% cut-off or 1–3 *pmoA* gene OTUs based on a 7% cut-off were observed in the intertidal marsh soil cores of the Yangtze Estuary, which were a bit higher than that of the DAMO bacteria in the sediments of Lake Constance (Deutzmann and Schink, 2011), Lake Biwa (Kojima et al., 2012), Xiazhuhu and Xixi wetlands (Hu et al., 2014a), and the paddy field (Hu et al., 2014a) where only one OTU was observed based on 7% differences. However, even higher *pmoA* gene OTU numbers were observed in the Qiantang River (1–9, 7% cut-off) (Shen et al., 2014a), Jiaojiang Estuary (1–8, 7% cut-off) (Shen et al., 2014b), and the Zhoushan islands (2–4, 7% cut-off) (Wang et al., 2019). According to previous studies, novel methanotroph species can be suggested when the *pmoA* gene nucleic acid sequence identity was lower than 93% compared to known species (Lüke and Frenzel, 2011). Our recovered *pmoA* cluster 2 only distantly related (88.5–89.7%) to the *pmoA* gene of *M. oxyfera* (Fig. 1), indicating that a potentially novel DAMO bacterial species reduces CH_4 emissions at the surface layer of the intertidal marsh soils.

Both the OTU numbers and the Shannon diversity of DAMO bacteria were higher at the surface layer than at the middle and soil-groundwater interface layers (Table 1), which might be due to the rhythmic material exchanges between land and sea in the intertidal marshes (Zheng et al., 2016). The intensive interaction between the Yangtze River freshwater and the coastal saline water might bring about diverse phylotypes to the surface layer of the intertidal soils (Zheng et al., 2016). In addition, the soil-tidal water interface might receive higher nutrient supply (Fig. S4), which can also support higher DAMO bacterial abundance. Indeed, the highest abundance of DAMO bacterial *pmoA* gene was observed at the surface layer of the soil cores (Fig. 3). The community structure of DAMO bacteria was different between the surface and soil-groundwater interface layers, though the UniFrac distances were not significant ($P > 0.05$) (Table S3). 90% of the *pmoA* sequences at the surface layer were grouped into cluster 2 in the constructed phylogenetic tree, while 88% and 100% of the *pmoA* clones at the middle and soil-groundwater interface layers, respectively, were affiliated to cluster 1 (Fig. 1). This result suggested that different genetypes of DAMO bacteria favor different environmental conditions, which was consistent with the previous finding that most of the habitats contained one certain *pmoA* OTU (Deutzmann and Schink, 2011; Hu et al., 2014a; Kojima et al., 2012).

So far, the occurrence and distribution of nitrate-DAMO archaea in the natural environments were quite rare, especially on the basis of the *mcrA* gene marker. However, in the intertidal environments, NO_3^- rather than NO_2^- is the main form of nitrogen oxides caused by human activities. Therefore, the significance of DAMO archaea and nitrate-DAMO process should be examined. In the present study, DAMO archaeal *mcrA* gene has been successfully detected in the intertidal marsh soils of the Yangtze Estuary. Based on a 3% divergence in nucleotides, 8 to 19 *mcrA* OTUs of the DAMO archaea were obtained, which were higher than the DAMO archaeal 16S rRNA gene OTU numbers obtained from Taihu lake (Ding et al., 2015), paddy soils (Ding et al., 2015), and the Zhoushan islands intertidal zone (Wang et al., 2019). In addition, the Shannon index of DAMO archaeal *mcrA* gene in intertidal marsh soil cores of the Yangtze Estuary (1.45–2.79) was higher than that of the DAMO archaeal 16S rRNA gene in the above ecosystems (0.14–1.73) (Ding et al., 2015; Wang et al., 2019). Furthermore, the observed DAMO archaeal biodiversity was significantly higher than that of the DAMO bacteria ($P < 0.05$) (Table 1). These results suggested that higher diverse of DAMO archaea might inhabit in the intertidal marsh soils of the Yangtze Estuary.

Unlike DAMO bacteria, higher diversity of DAMO archaea was also detected at the soil-groundwater interface (Table 1). We hypothesized that the higher DAMO archaeal diversity at the deep soil layer might be caused by the influence of the groundwater. It has been reported that tidal dynamics in the intertidal zone can induce periodic fluctuations of the groundwater table (Santos et al., 2012; Zheng et al., 2016), which can bring about pulsed input of groundwater-transported materials as well as diverse DAMO archaea into deeper soil. However, the deep soil layer was not characterized by higher DAMO archaeal abundance and activity (Fig. 3 and 4), which might be due to the metabolic inhibition by the groundwater-derived O_2, as the shallow coastal aquifers are typically micro-oxic (Tobias et al., 2001). The community composition of DAMO archaea also showed the micro-niche variations along the soil profile (Fig. 2), although the community differences were not

significant based on the UniFrac distance matrix (Table S3). These results suggested that the community structure, diversity, and distribution of DAMO archaea might be affected by the tidal dynamics which mold the vertical distribution pattern of the micro-ecological conditions (Kuwae et al., 2003).

The qPCR results showed that the copy number of DAMO bacterial *pmoA* gene ranged from 8.2×10^5 to 3.0×10^7 copies g^{-1} in the intertidal soil cores of the Yangtze Estuary, which were approximate to that of the mangrove sediments (2.1×10^6–3.4×10^7 copies g^{-1} dry sediment) (Zhang et al., 2018). In addition, the results were also approximate to the abundance of DAMO bacteria based on the 16S rRNA gene analyses in the Hangzhou Bay (5.4×10^6–5.0×10^7 copies g^{-1} dry soil) (Shen et al., 2016), Xiazhuhu wetland (3.0×10^6–3.2×10^7 copies g^{-1} dry soil) (Hu et al., 2014a), Xixi wetland (1.7×10^6–1.0×10^7 copies g^{-1} dry soil) (Hu et al., 2014a), paddy field (1.5×10^6–4.5×10^6 copies g^{-1} dry soil) (Hu et al., 2014a), and the Qiantang River (1.32×10^6–1.03×10^7 copies g^{-1} dry soil) (Shen et al., 2014a) (Table S4). This comparison suggested that the abundance of DAMO bacteria in the natural environment obtained with the *pmoA* gene primers was consistent with that obtained with the 16S rRNA gene primers. The copy number of DAMO archaeal *mcrA* gene in the intertidal soil cores of the Yangtze Estuary was 3.0×10^5–3.9×10^7 copies g^{-1}, which were relatively higher than that retrieved from the paddy soil (7.2×10^3–1.8×10^7 copies g^{-1} dry soil) (Vaksmaa et al., 2017a, 2017b), river sediment (3.0×10^4–4.4×10^5 copies g^{-1} wet sediment) (Vaksmaa et al., 2017a), and the North Sea sediment (2.5×10^4 copies g^{-1} wet sediment) (Vaksmaa et al., 2017a). Previous studies showed that the abundance of DAMO archaea in the environmental samples obtained with the 16S rRNA gene primers was approximately two orders of magnitude higher than that obtained with the *mcrA* primers (Vaksmaa et al., 2017a). Therefore, the number of DAMO archaea might be overestimated based on 16S rRNA gene primers, which were less specific for DAMO archaea than *mcrA* gene (Vaksmaa et al., 2017a). It was the reason why *mcrA* was used as the gene marker to quantify the abundance of DAMO archaea in the present study.

Our data also indicated that the DAMO bacteria and archaea were present together in the intertidal zone, showing that there might be an intimate symbiotic relationship between the two microorganisms (Wang et al., 2019). However, the relative abundance of DAMO bacteria and archaea showed a vertical stratification along the soil cores, with more abundant DAMO bacteria at the soil-tidal water interface as well as at the soil-groundwater interface, while DAMO archaea tended to be more abundant than DAMO bacteria at the middle layers (Fig. S7a). We speculated that it might be attributed to the different preference of DAMO bacteria and archaea for oxygen, as DAMO archaea preferred a more anoxic environment (Wang et al., 2019). The tidal water and groundwater might bring about trace amount of oxygen to the upper and deep soil layers, which was confirmed by the vertical distribution pattern of the soil Eh (Fig. S4). In fact, a significant correlation was observed between the ratio of *pmoA* abundance/*mcrA* abundance and Eh in the intertidal marsh soils of the Yangtze Estuary (Fig. S10). Furthermore, a similar vertical distribution pattern was also observed for the relative contributions of DAMO bacteria and archaea to anaerobic CH_4 oxidation (Fig. S7b).

It was interesting to find that the middle layer of the soil cores, at which the NO_3^- concentration was low, harbored the highest abundance of DAMO archaea, though with the lowest diversity. This might support the hypothesis that DAMO archaea can use diverse electron acceptors to anaerobically oxidize CH_4 in addition to NO_3^- (Ettwig et al., 2016). *M. nitroreducens*-like DAMO archaea was reported to have the ability to oxidize CH_4 using Fe(III) (Ettwig et al., 2016), and it was recently observed that the addition of Fe(III) stimulated the expression of DAMO archaeal *mcrA* gene (Shen et al., 2019). In addition, it was evidenced that the ANME-2d archaea were also involved in sulfate-AOM in lake sediments based on RNA stable isotope probing (RNA-SIP) incubation experiments (Weber et al., 2017). Thus, it was possible that the abundant DAMO archaea were co-supported by different electron acceptors besides NO_3^-. However, there were no significant correlations of DAMO archaeal *mcrA* gene abundance with the contents of individual electron acceptors of NO_3^-, Fe(III), and SO_4^{2-} in the intertidal marsh soils in the present study ($P > 0.05$) (Table S2). Furthermore, the possibility that DAMO archaea perform natural organic matter-dependent anaerobic CH_4 oxidation in intertidal marsh soils cannot be excluded (Valenzuela et al., 2017, 2019), although the relationship between the abundance of DAMO archaea and soil OC content was not significant ($P > 0.05$) (Table S2).

The potential nitrite-DAMO activity measured in this study ranged from 0.1 to 3.8 nmol $^{13}CO_2$ g^{-1} dry soil day^{-1} (Fig. 4), which was approximate to that reported from the Xiazhuhu wetland (0.31–5.43 $^{13}CO_2$ g^{-1} dry soil day^{-1}) (Hu et al., 2014a), Xixi wetland (0.68–4.92 $^{13}CO_2$ g^{-1} dry soil day^{-1}) (Hu et al., 2014a), paddy fields (1.68–2.04 $^{13}CO_2$ g^{-1} dry soil day^{-1}) (Hu et al., 2014a), and the East China Sea intertidal zone (0.5–5.7 $^{13}CO_2$ g^{-1} dry soil day^{-1}) (Wang et al., 2017), but slightly higher than that from the Zhoushan Island (0–1.51 $^{13}CO_2$ g^{-1} dry soil day^{-1}) (Wang et al., 2019) and the Hangzhou Bay (0.2–1.3 $^{13}CO_2$ g^{-1} dry soil day^{-1}) (Shen et al., 2016) (Table S5). However, even higher nitrite-DAMO rate was reported in the reduced riverbeds (0.4–61.0 $^{13}CO_2$ g^{-1} dry soil day^{-1}) (Shen et al., 2019) and the mangrove sediments (25.9–704.1 $^{13}CO_2$ g^{-1} dry sediment day^{-1}) (Zhang et al., 2018). The potential nitrate-DAMO activity measured in this study varied from 0.1 to 4.1 nmol $^{13}CO_2$ g^{-1} dry soil day^{-1} (Fig. 4), which was slightly higher than that measured in the Zhoushan Island (0–1.57 nmol $^{13}CO_2$ g^{-1} dry soil day^{-1}) (Table S5). The cell-specific activities for DAMO bacteria estimated in the present study (average of 0.3 fmol $^{13}CO_2$ $cell^{-1}$ day^{-1}) were approximate to the reported values, 0.28–0.34 fmol CH_4 $cell^{-1}$ day^{-1} estimated for enrichment cultures with 16S rRNA gene-targeted primers qP1F/qP1R (Hu et al., 2014b). Relatively lower activities, 0.09 and 0.11 fmol CH_4 $cell^{-1}$ day^{-1} were also assessed for enrichment cultures with qP1F/qP1R (Ettwig et al., 2009; Zhu et al., 2011). However, significantly higher cell-specific activity for DAMO bacteria (0.8–335.3 fmol $^{13}CO_2$ $cell^{-1}$ day^{-1}) was estimated in mangrove sediments with the same *pmoA* primers as we used (Zhang et al., 2018). Furthermore, the cell-specific methane oxidation rates for DAMO archaea estimated in the present study (average of 0.2 fmol $^{13}CO_2$ $cell^{-1}$ day^{-1}) were comparable to those reported for enrichment cultures (0.57 fmol $^{13}CO_2$ $cell^{-1}$ day^{-1}) from paddy field soils with 16S rRNA gene-targeted primers (Vaksmaa et al., 2017c). These comparisons were based on the assumptions that each genome contained one *pmoA*/*mcrA*/16S rRNA gene copy, the molar ratio of CO_2 generation and CH_4 conversion was the theoretical 1:1, and all obtained microbial sequences derived from active microbes.

It should be noted that, the measured nitrite-DAMO rate in group b (amended with $^{13}CH_4 + NO_2^-$) might be higher than that in group c (amended with $^{13}CH_4 + NO_3^-$), as NO_2^- for DAMO bacteria in group c was provided indirectly as the end product of nitrate-DAMO process or intermediate product of denitrification. The produced NO_2^- was thus probably not sufficient enough to support the anaerobic CH_4 oxidation capacity of DAMO bacteria. Therefore, the potential nitrate-DAMO rate might be underestimated. In the present study, we observed that the potential DAMO rate increased with an increasing addition of NO_3^- from 0.5 mM to 5 mM, while it remained relatively stable with even higher NO_3^- additions (Fig. S2). It was the reason why 5 mM NO_3^- was added to estimate the DAMO potential of the intertidal marsh soils. This also suggested that the added NO_3^- was sufficient to support the DAMO potential and the produced NO_2^- by DAMO archaea and denitrifiers might also be enough for DAMO bacteria to oxidize CH_4. Thus, the possible underestimation of the nitrate-DAMO potential might be not significant here. Moreover, given that NO_3^- is typically far more abundant than NO_2^- in the intertidal marshes, it is reasonable to use the DAMO potential measured with $^{13}CH_4 + NO_3^-$ to estimate the potential role of both DAMO bacteria and archaea in attenuating CH_4 emissions from intertidal marsh soils.

Though sulfate-AOM was the main CH_4 removal pathway in marine habitats (Knittel and Boetius, 2009), it was observed that the contribution of DAMO to CH_4 sink was greater than that of sulfate-AOM in the Zhoushan intertidal zone (Wang et al., 2019). Here, the measured potential DAMO rate in the intertidal marsh soils of the Yangtze Estuary (0.3–7.0 nmol $^{13}CO_2$ g^{-1} dry soil day^{-1}) was significantly higher than the observed sulfate-AOM rate (0–0.74 nmol $^{13}CO_2$ g^{-1} dry soil day^{-1}) in the Zhoushan intertidal zone (Wang et al., 2019), indicating that the DAMO process was an important CH_4 sink which was previously overlooked in coastal ecosystems. Moreover, the standard Gibbs free energies for nitrite-dependent (-928 kJ mol^{-1}) and nitrate-dependent (-519.8 kJ mol^{-1}) anaerobic oxidation of CH_4 are greater than those for sulfate-dependent (-16.6 kJ mol^{-1}) and ferric iron-dependent (-81.6 kJ mol^{-1}) anaerobic oxidation of CH_4 (Shen et al., 2019). Thus, denitrifying methanotrophs are energetically more favorable, and may have an advantage of using CH_4 over the sulfate- and ferric iron-dependent methanotrophs in the natural environments where NO_2^-/NO_3^-, SO_4^{2-} and Fe(III) coexist, such as the intertidal marshes. A significant negative correlation between the DAMO rate and CH_4 content in soil pore water was observed (Fig. 5), further implying that DAMO process might play an important role in consuming CH_4. It should be noted that, some aerobic methanotrophs can also use NO_2^-/NO_3^- as the alternative electron acceptors under oxygen limitation (Kits et al., 2015), thus they may also play a role in the DAMO potential here.

In the examined soil cores, the surface layer was the main habitat for denitrifying methanotrophic activity (Fig. 4), which might be attributed to the diffusive input of NO_2^-/NO_3^- from overlying tidal water (Deng et al., 2014). Likewise, in the mangrove sediment of the Zhangjiang Estuary, nitrite-DAMO bacteria was also more active and more abundant at the upper layer (0–20 cm) (Zhang et al., 2018). In contrast, it was found that the potential nitrite-DAMO activity at the deeper layers (90–100 cm) was much higher than at the upper layer (20–30 cm) in paddy fields (Hu et al., 2014a). In the present study, nitrite-DAMO activity also showed some recovery at around 100 cm soil depth, which might be due to the influence of the groundwater. According to our previous study, denitrification was greatly enhanced at the soil-groundwater interface in the intertidal marshes, due to the effect of tidal pumping (Zheng et al., 2016). Thus, the enhanced activity of denitrifiers might provide more NO_2^- and facilitate the activity of DAMO bacteria at this deep layer. However, no significant correlation was observed between the rate of denitrification and nitrite-DAMO in the whole intertidal soil cores (Fig. S11). Moreover, the potential DAMO rate was also peaked at the 45–50 cm soil depth (Fig. 4a), mainly due to the enhanced potential activity of DAMO archaea (Fig. 4b).

In the present study, NO_3^- and SO_4^{2-} showed significant correlations with the abundance of DAMO bacteria in the intertidal marsh soils ($P < 0.01$) (Fig. 5), which was consistent with the previous finding that high NO_3^- concentration was more suitable for the growth of DAMO bacteria (Shen et al., 2016). Therefore, the high NO_3^- concentration is not only beneficial for the growth of DAMO archaea but also makes it possible for DAMO bacteria to grow (Wang et al., 2019). However, in the present study, no significant correlation was observed between the abundances of DAMO bacteria and DAMO archaea in the intertidal marsh soil cores ($P > 0.05$), further suggesting that nitrate-DAMO was not the only NO_2^- providing pathway for DAMO bacteria, and the symbiotic relationship between them might also be influenced by tidal dynamics.

Based on the stoichiometric relationship between CH_4 and NO_2^- in the DAMO reaction (3,8, Ettwig et al., 2010) and the measured nitrite-DAMO rate in the present study, it was estimated that the potential nitrogen removal rate during nitrite-DAMO ranged between 0.4 and 10.1 nmol N g^{-1} dry soil day^{-1} (Fig. S9). According to our previous research in the study area, the nitrogen removal rates in the intertidal soil cores ranged from 3.9 to 14.6 nmol N g^{-1} dry soil day^{-1} for denitrification and 23.8–187.2 nmol N g^{-1} dry soil day^{-1} for anammox (Zheng et al., 2016; Fig. S12). Based on these results, the potential contribution of nitrite-DAMO process to total N_2 production at the study site was estimated to be approximately 7% (the mean depth-integrated contribution) as compared to denitrification and anammox (Fig. S12). This result suggested that in addition to playing an important role in CH_4 sink, the DAMO process was also a non-negligible pathway of nitrogen removal from the intertidal marshes.

5. Conclusions

The co-occurrence and stratification of the nitrite- and nitrate-dependent DAMO bioprocesses in the intertidal marsh soil cores of the Yangtze Estuary was evidenced. Based on the functional gene markers of *pmoA* and *mcrA,* DAMO bacteria and archaea were successfully detected, and their community composition and diversity exhibited vertical differences with soil depth. The average abundance of DAMO bacteria was similar to that of DAMO archaea in the intertidal marsh soils, whereas the biodiversity of DAMO archaea was significantly higher than that of DAMO bacteria. In the intertidal marsh soils, the average contribution of DAMO bacteria to CH_4 oxidation during the DAMO process was slightly higher than that of DAMO archaea. Due to the influence of tidal dynamics, both the abundance and activity of DAMO bacteria tended to be higher than those of DAMO archaea at the soil-tidal water interface and soil-groundwater interface layers, whereas DAMO archaea tended to play a more important role at the middle layers. These results suggested new insights about how DAMO bacteria and archaea interact in an intertidal environment subjected to periodic tidal inundation and exposure, and demonstrated their environmental significance in the intertidal marshes. Future work is needed to compare the role of DAMO with CH_4 oxidation potentials driven by other electron accepters in intertidal marsh soils.

Declaration of competing interest

None.

Acknowledgements

This work was funded by Chinese National Key Programs for Fundamental Research and Development (2016YFA0600904) and National Natural Science Foundation of China (Nos. 41601530, 41725002, 41671463, 41761144062, and 41730646). We also thank the support of the Yangtze Delta Estuarine Wetland Station, East China Normal University. Gene sequence data in this paper can be downloaded from GenBank with accession number MK887934-MK888208, and other data can be obtained by sending a written request to the corresponding author.

Appendix A. Supplementary data

Supplementary data to this article can be found online at https://doi.org/10.1016/j.geoderma.2019.113943.

References

Ajwa, H.A., Tabatabai, M.A., 1993. Comparison of some methods for determination of sulfate in soils. Commun. Soil Sci. Plan. 24, 1817–1832.
Bastviken, D., Tranvik, L.J., Downing, J.A., Crill, P.M., Enrich-Prast, A., 2011. Freshwater methane emissions offset the continental carbon sink. Science 331, 50.
Beal, E.J., House, C.H., Orphan, V.J., 2009. Manganese- and iron-dependent marine methane oxidation. Science 325, 184–187.
Canfield, D.E., Glazer, A.N., Falkowski, P.G., 2010. The evolution and future of earth's nitrogen cycle. Science 330, 192–196.
Caporaso, J.G., Kuczynski, J., Stombaugh, J., Bittinger, K., Bushman, F.D., Costello, E.K., Fierer, N., Pena, A.G., Goodrich, J.K., Gordon, J.I., Huttley, G.A., Kelley, S.T., Knights, D., Koenig, J.E., Ley, R.E., Lozupone, C.A., McDonald, D., Muegge, B.D., Pirrung, M., Reeder, J., Sevinsky, J.R., Turnbaugh, P.J., Walters, W.A., Widmann, J., Yatsunenko, T., Zaneveld, J., Knight, R., Peña, A.G., Goodrich, J.K., Gordon, J.I., Huttley, G.A., Kelley, S.T., Knights, D., Koenig, J.E., Ley, R.E., Lozupone, C.A.,

McDonald, D., Muegge, B.D., Pirrung, M., Reeder, J., Sevinsky, J.R., Turnbaugh, P.J., Walters, W.A., Widmann, J., Yatsunenko, T., Zaneveld, J., Knight, R., 2010. QIIME allows analysis of high-throughput community sequencing data. Nat. Methods 7, 335–336.

Chen, J., Zhou, Z.C., Gu, J.D., 2014. Occurrence and diversity of nitrite-dependent anaerobic methane oxidation bacteria in the sediments of the South China Sea revealed by amplification of both 16S rRNA and *pmoA* genes. Appl. Microbiol. Biotechnol. 98, 5685–5696.

Dean, J.F., Middelburg, J.J., Röckmann, T., Aerts, R., Blauw, L.G., Egger, M., Jetten, M.S.M, de Jong, A.E.E., Meisel, O.H., Rasigraf, O., Slomp, C.P., 2018. Methane feedbacks to the global climate system in a warmer world. t Zandt, M.H., Dolman, A.J. (Eds.), Rev. Geophys. 56, 207–250.

Deng, H.G., Wang, D.Q., Chen, Z.L., Liu, J., Xu, S.Y., White, J.R., 2014. Vertical dissolved inorganic nitrogen fluxes in marsh and mudflat areas of the Yangtze Estuary. J. Environ. Qual. 43, 745–752.

Deng, Y.C., Cui, X.Y., Dumont, M.G., 2016. Identification of active aerobic methanotrophs in plateau wetlands using DNA stable isotope probing. FEMS Microbiol. Lett. 363, 168.

Deutzmann, J.S., Schink, B., 2011. Anaerobic oxidation of methane in sediments of lake constance, an oligotrophic freshwater lake. Appl. Environ. Microbiol. 77, 4429–4436.

Ding, J., Ding, Z.W., Fu, L., Lu, Y.Z., Cheng, S.H., Zeng, R.J., 2015. New primers for detecting and quantifying denitrifying anaerobic methane oxidation archaea in different ecological niches. Appl. Microbiol. Biotechnol. 99, 9805–9812.

Ettwig, K.F., Shima, S., van de Pas-Schoonen, K.T., Kahnt, J., Medema, M.H., den Camp, Op, Jetten, M.S.M., Strous, M., 2008. Denitrifying bacteria anaerobically oxidize methane in the absence of archaea. Environ. Microbiol. 10, 3164–3173.

Ettwig, K.F., van Alen, T., van de Pas-Schoonen, K.T., Jetten, M.S.M., Strous, M., 2009. Enrichment and molecular detection of denitrifying methanotrophic bacteria of the NC10 phylum. Appl. Environ. Microbiol. 75, 3656–3662.

Ettwig, K.F., Butler, M.K., Paslier, D.L., Pelletier, E., Mangenot, S., Kuypers, M.M.M., Schreiber, F., Dutilh, B.E., Zedelius, J., de Beer, D., Gloerich, J., Wessels, H.J.C.T., van Alen, T., Luesken, F., Wu, M.L., van de Pas-Schoonen, K.T., Op den Camp, H.J.M., Janssen-Megens, E.M., Francoijs, K.J., Stunnenberg, H., Weissenbach, J., Jetten, M.S.M., Strous, M., 2010. Nitrite-driven anaerobic methane oxidation by oxygenic bacteria. Nature 464, 543–548.

Ettwig, K.F., Zhu, B., Speth, D., Keltjens, J.T., Jetten, M.S.M., Kartal, B., 2016. Archaea catalyze iron-dependent anaerobic oxidation of methane. Proc. Natl. Acad. Sci. U. S. A. 113, 12792–12796.

Haese, R.R., Wallmann, K., Dahmke, A., Kretzmann, U., Müller, P.J., Schulz, H.D., 1997. Iron species determination to investigate early diagenetic reactivity in marine sediments. Geochim. Cosmochim. Ac. 61, 63–72.

Haroon, M.F., Hu, S., Shi, Y., Imelfort, M., Keller, J., Hugenholtz, P., Yuan, Z., Tyson, G.W., 2013. Anaerobic oxidation of methane coupled to nitrate reduction in a novel archaeal lineage. Nature 500, 567–570.

He, Z., Cai, C., Wang, J., Xu, X., Ping, Z., Jetten, M.S.M., Hu, B., 2016a. A novel denitrifying methanotroph of the NC10 phylum and its microcolony. Sci. Rep. 6, 32241.

He, Z., Wang, J., Hu, J., Zhang, H., Cai, C., Shen, J., Xu, X., Zheng, P., Hu, B., 2016b. Improved PCR primers to amplify 16S rRNA genes from NC10 bacteria. Appl. Microbiol. Biotechnol. 100, 5099–5108.

Hou, L.J., Zheng, Y.L., Liu, M., Gong, J., Zhang, X.L., Yin, G.Y., You, L.L., 2013. Anaerobic ammonium oxidation (anammox) bacterial diversity, abundance, and activity in marsh sediments of the Yangtze estuary. J. Geophys. Res. Biogeosci. 118, 1237–1246.

Hu, B.L., Shen, L.D., Lian, X., Zhu, Q., Liu, S., Huang, Q., He, Z.F., Geng, S., Cheng, D.Q., Lou, L.P., Xu, X.Y., Zheng, P., He, Y.F., 2014a. Evidence for nitrite-dependent anaerobic methane oxidation as a previously overlooked microbial methane sink in wetlands. Proc. Natl. Acad. Sci. U. S. A. 111, 4495–4500.

Hu, B.L., He, Z.F., Geng, S., Cai, C., Lou, L.P., Zheng, P., Xu, X.H., 2014b. Cultivation of nitrite-dependent anaerobic methane-oxidizing bacteria: impact of reactor configuration. Appl. Microbiol. Biotechnol. 98, 7983–7991.

Hu, S., Zeng, R.J., Haroon, M.F., Keller, J., Lant, P.A., Tyson, G.W., Yuan, Z.G., 2015. A laboratory investigation of interactions between denitrifying anaerobic methane oxidation (DAMO) and anammox processes in anoxic environments. Sci. Rep. 5, 8706.

Kintisch, E., 2013. Can coastal marshes rise above it all? Science 341, 480–481.

Kits, K.D., Klotz, M.G., Stein, L.Y., 2015. Methane oxidation coupled to nitrate reduction under hypoxia by the Gammaproteobacterium *Methylomonas denitrificans*, sp. nov. type strain FJG1. Environ. Microbiol. 17, 3219–3232.

Knittel, K., Boetius, A., 2009. Anaerobic oxidation of methane: progress with an unknown process. Annu. Rev. Microbiol. 63, 311–334.

Kojima, H., Tsutsumi, M., Ishikawa, K., Iwata, T., Mußmann, M., Fukui, M., 2012. Distribution of putative denitrifying methane oxidizing bacteria in sediment of a freshwater lake, Lake Biwa. Syst. Appl. Microbiol. 35, 233–238.

Kumar, S., Stecher, G., Tamura, K., 2016. MEGA7: molecular evolutionary genetics analysis version 7.0 for bigger datasets. Mol. Biol. Evol. 33, 1870–1874.

Kuwae, T., Kibe, E., Nakamura, Y., 2003. Effect of emersion and immersion on the porewater nutrient dynamics of an intertidal sandflat in Tokyo Bay. Estuar. Coast. Shelf Sci. 57, 929–940.

Long, Y., Jiang, X.J., Guo, Q.W., Li, B.X., Xie, S.G., 2017. Sediment nitrite-dependent methane-oxidizing microorganisms temporally and spatially shift in the Dongjiang River. Appl. Microbiol. Biotechnol. 101, 401–410.

Luesken, F.A., Zhu, B.L., van Alen, T.A., Butler, M.K., Rodriguez Diaz, M., Song, B.K., Op den Camp, H.J.M., Jetten, M.S.M., Ettwig, K.F., 2011. *pmoA* primers for detection of anaerobic methanotrophs. Appl. Environ. Microbiol. 77, 3877–3880.

Lüke, C., Frenzel, P., 2011. Potential of *pmoA* amplicon pyrosequencing for methanotroph diversity studies. Appl. Environ. Microbiol. 77, 6305–6309.

Mohamed, N.M., Saito, K., Tal, Y., Hill, R.T., 2010. Diversity of aerobic and anaerobic ammonia-oxidizing bacteria in marine sponges. ISME J 4, 38–48.

Myhre, G., Shindell, D., Bréon, F.M., Collins, W., Fuglestvedt, J., Huang, J., Koch, D., Lamarque, J.F., Lee, D., Mendoza, B., Nakajima, T., Robock, A., Stephens, G., Takemura, T., Zhang, H., 2013. Anthropogenic and natural radiative forcing. In: Climate Change 2013: The Physical Science Basis. Contribution of Working Group I to the Fifth Assessment Report of the Intergovernmental Panel on Climate Change. Cambridge University Press, Cambridge.

Padilla, C.C., Bristow, L.A., Sarode, N., Garcia-Robledo, E., Gomez Ramirez, E., Benson, C.R., Bourbonnais, A., Altabet, M.A., Girguis, P.R., Thamdrup, B., Stewart, F.J., 2016. NC10 bacteria in marine oxygen minimum zones. ISME J 10, 2067–2071.

Raghoebarsing, A.A., Pol, A., Van de Pas-Schoonen, K.T., Smolders, A.J.P., Ettwig, K.F., Rijpstra, W.I.C., Schouten, S., Sinninghe Damsté, J.S., Op den Camp, H.J.M., Jetten, M.S.M., Strous, M., 2006. A microbial consortium couples anaerobic methane oxidation to denitrification. Nature 440, 918–921.

Rios-Del Toro, E.E., Valenzuela, E.I., Ramírez, J.E., López-Lozano, N.E., Cervantes, F.J., 2018. Anaerobic ammonium oxidation linked to microbial reduction of natural organic matter in marine sediments. Environ. Sci. Technol. Lett. 5, 571–577.

Roussel, E.G., Sauvadet, A.L., Allard, J., Chaduteau, C., Richard, P., Cambon Bonavita, M.A., Chaumillon, E., 2009. Archaeal methane cycling communities associated with gassy subsurface sediments of Marennes-Oleron Bay (France). Geomicrobiol J. 26, 31–43.

Santos, I.R., Eyre, B.D., Huettel, M., 2012. The driving forces of porewater and groundwater flow in permeable coastal sediments: a review. Estuar. Coast. Shelf Sci. 98, 1–15.

Schloss, P.D., Westcott, S.L., Ryabin, T., Hall, J.R., Hartmann, M., Hollister, E.B., Lesniewski, R.A., Oakley, B.B., Parks, D.H., Robinson, C.J., Sahl, J.W., Stres, B., Thallinger, G.G., Van Horn, D.J., Weber, C.F., 2009. Introducing mothur: open-source, platform-independent, community-supported software for describing and comparing microbial communities. Appl. Environ. Microbiol. 75, 7537–7541.

Schwietzke, S., Sherwood, O.A., Bruhwiler, L.M.P., Miller, J.B., Etiope, G., Dlugokencky, E.J., Michel, S.E., Arling, V.A., Vaughn, B.H., White, J.W.C., Tans, P.P., 2016. Upward revision of global fossil fuel methane emissions based on isotope database. Nature 538, 88–91.

Segarra, K.E.A., Comerford, C., Slaughter, J., Joye, S.B., 2013. Impact of electron acceptor availability on the anaerobic oxidation of methane in coastal freshwater and brackish wetland sediments. Geochim. Cosmochim. Acta 115, 15–30.

Shen, L.D., Liu, S., Zhu, Q., Li, X.Y., Cai, C., Cheng, D.Q., Lou, L.P., Xu, X.Y., Zheng, P., Hu, B.L., 2014a. Distribution and diversity of nitrite-dependent anaerobic methane-oxidising bacteria in the sediments of the Qiantang River. Microb. Ecol. 67, 341–349.

Shen, L.D., Zhu, Q., Liu, S., Du, P., Zeng, J.N., Cheng, D.Q., Xu, X.Y., Zheng, P., Hu, B.L., 2014b. Molecular evidence for nitrite-dependent anaerobic methane oxidizing bacteria in the Jiaojiang Estuary of the East Sea (China). Appl. Microbiol. Biotechnol. 98, 5029–5038.

Shen, L.D., Huang, Q., He, Z., Lian, X., Liu, S., He, Y.F., Lou, L.P., Xu, X.Y., Zheng, P., Hu, B.L., 2015. Vertical distribution of nitrite-dependent anaerobic methane-oxidizing bacteria in natural freshwater wetland soils. Appl. Microbiol. Biotechnol. 99, 349–357.

Shen, L.D., Hu, B.L., Liu, S., Chai, X.P., He, Z.F., Ren, H.X., Liu, Y., Geng, S., Wang, W., Tang, J.L., Wang, Y.M., Lou, L.P., Xu, X.Y., Zheng, P., 2016. Anaerobic methane oxidation coupled to nitrite reduction can be a potential methane sink in coastal environments. Appl. Microbiol. Biotechnol. 100, 7171–7180.

Shen, L.D., Ouyang, L., Zhu, Y.Z., Trimmer, M., 2019. Active pathways of anaerobic methane oxidation across contrasting riverbeds. ISME J 13, 752–766.

Sultana, N., Zhao, J., Zheng, Y., Cai, Y.F., Faheem, M., Peng, X.L., Wang, W.D., Jia, Z.J., 2019. Stable isotope probing of active methane oxidizers in rice field soils from cold regions. Biol. Fertil. Soils 55, 243–250.

Tobias, C.R., Anderson, I.C., Canuel, E.A., Macko, S.A., 2001. Nitrogen cycling through a fringing marsh-aquifer ecotone. Mar. Ecol. Prog. Ser. 210, 25–39.

Urish, D.W., McKenna, T.E., 2004. Tidal effects on ground water discharge through a sandy marine beach. Ground Water 42, 971–982.

Vaksmaa, A., Jetten, M.S.M., Ettwig, K.F., Lüke, C., 2017a. *McrA* primers for the detection and quantification of the anaerobic archaeal methanotroph '*Candidatus* Methanoperedens nitroreducens'. Appl. Microbiol. Biotechnol. 101, 1631–1641.

Vaksmaa, A., van Alen, T.A., Ettwig, K.F., Lupotto, E., Valè, G., Jetten, M.S.M., Lüke, C., 2017b. Stratification of diversity and activity of mthanogenic and methanotrophic microorganisms in a nitrogen-fertilized Italian paddy soil. Front. Microbiol. 8, 2127.

Vaksmaa, A., Guerrero-Cruz, S., van Alen, T.A., Cremers, G., Ettwig, K.F., Lüke, C., Jetten, M.S.M., 2017c. Enrichment of anaerobic nitrate-dependent methanotrophic '*Candidatus* Methanoperedens nitroreducens' archaea from an Italian paddy field soil. Appl. Microbiol. Biotechnol. 101, 7075–7084.

Valenzuela, E.I., Prieto-Davó, A., López-Lozano, N.E., Hernández-Eligio, A., Vega-Alvarado, L., Juárez, K., García-González, A.S., López, M.G., Cervantes, F.J., 2017. Anaerobic methane oxidation driven by microbial reduction of natural organic matter in a tropical wetla. Appl. Environ. Microbiol. 83 e00645-17.

Valenzuela, E.I., Avendaño, K.A., Balagurusamy, N., Arriaga, S., Nieto-Delgado, C., Thalasso, F., Cervantes, F.J., 2019. Electron shuttling mediated by humic substances fuels anaerobic methane oxidation and carbon burial in wetland sediments. Sci. Total Environ. 650, 2674–2684.

Wallmann, K., Hennies, K., König, I., Petersen, W., Knauth, H.D., 1993. New procedure for determining reactive Fe(III) and Fe(II) minerals in sediments. Limnol. Oceanogr. 38, 1803–1812.

Wang, J.Q., Shen, L.D., He, Z.F., Hu, J.J., Cai, Z.Y., Zheng, P., Hu, B.L., 2017. Spatial and temporal distribution of nitrite-dependent anaerobic methane-oxidizing bacteria in an intertidal zone of the East China Sea. Appl. Microbiol. Biotechnol. 101, 8007–8014.

Wang, J.Q., Cai, C.Y., Li, Y.F., Hua, M.L., Wang, J.R., Yang, H.R., Zheng, P., Hu, B.L.,

2019. Denitrifying anaerobic methane oxidation: a previously overlooked methane sink in intertidal zone. Environ. Sci. Technol. 53, 203–212.
Wang, P.L., Chiu, Y.P., Cheng, T.W., Chang, Y.H., Tu, W.X., Lin, L.H., 2014. Spatial variations of community structures and methane cycling across a transect of Lei-Gong-Hou mud volcanoes in eastern Taiwan. Front. Microbiol. 5, 121.
Weber, H.S., Habicht, K.S., Thamdrup, B., 2017. Anaerobic methanotrophic archaea of the ANME-2d cluster are active in a low-sulfate, iron-rich freshwater sediment. Front. Microbiol. 8, 619.
Welte, C.U., Rasigraf, O., Vaksmaa, A., Versantvoort, W., Arshad, A., Op den Camp, H.J.M., Jetten, M.S.M., Lüke, C., Reimann, J., 2016. Nitrate- and nitrite-dependent anaerobic oxidation of methane. Env. Microbiol. Rep. 8, 941–955.
Winkel, M., Mitzscherling, J., Overduin, P.P., Horn, F., Winterfeld, M., Rijkers, R., Grigoriev, M.N., Knoblauch, C., Mangelsdorf, K., Wagner, D., Liebner, S., 2018. Anaerobic methanotrophic communities thrive in deep submarine permafrost. Sci. Rep. 8, 1291.
Zhang, M.P., Luo, Y., Lin, L.A., Lin, X.L., Hetharua, B., Zhao, W.J., Zhou, M.K., Zhan, Q., Xu, H., Zheng, T.L., Tian, Y., 2018. Molecular and stable isotopic evidence for the occurrence of nitrite-dependent anaerobic methane-oxidizing bacteria in the mangrove sediment of Zhangjiang Estuary, China. Appl. Microbiol. Biotechnol. 102, 2441–2454.
Zheng, Y.L., Hou, L.J., Newell, S., Liu, M., Zhou, J.L., Zhao, H., You, L.L., Cheng, X.L., 2014. Community dynamics and activity of ammonia-oxidizing prokaryotes in intertidal sediments of the Yangtze Estuary. Appl. Environ. Microbiol. 80, 408–419.
Zheng, Y.L., Hou, L.J., Liu, M., Liu, Z.F., Li, X.F., Lin, X.B., Yin, G.Y., Gao, J., Yu, C.D., Wang, R., Jiang, X.F., 2016. Tidal pumping facilitates dissimilatory nitrate reduction in intertidal marshes. Sci. Rep. 6, 21338.
Zhou, L.L., Wang, Y., Long, X.E., Guo, J.H., Zhu, G.B., 2014. High abundance and diversity of nitrite-dependent anaerobic methane-oxidizing bacteria in a paddy field profile. FEMS Microbiol. Lett. 360, 33–41.
Zhu, B., Sanchez, J., van Alen, T.A., Sanabria, J., Jetten, M.S.M., Ettwig, K.F., Kartal, B., 2011. Combined anaerobic ammonium and methane oxidation for nitrogen and methane removal. Biochem. Soc. Trans. 39, 1822–1825.